THE JOURNAL OF PHYSICAL CHEMISTRY B

Article

pubs.acs.org/JPCB

Characterization of the Thermal and Photoinduced Reactions of Photochromic Spiropyrans in Aqueous Solution

Martin Hammarson, Jesper R. Nilsson, Shiming Li, Tamás Beke-Somfai, and Joakim Andréasson*

Department of Chemical and Biological Engineering, Physical Chemistry, Chalmers University of Technology, 412 96 Göteborg, Sweden

Supporting Information

ABSTRACT: Six water-soluble spiropyran derivatives have been characterized with respect to the thermal and photoinduced reactions over a broad pH-interval. A comprehensive kinetic model was formulated including the spiro- and the merocyanine isomers, the respective protonated forms, and the hydrolysis products. The experimental studies on the hydrolysis reaction mechanism were supplemented by calculations using quantum mechanical (QM) models employing density functional theory. The results show that (1) the substitution pattern dramatically influences the pK_a-values of the protonated forms as well as the rates of the thermal isomerization reactions, (2) water is the nucleophile in the hydrolysis reaction around neutral pH, (3) the phenolate oxygen of the merocyanine form plays a key role in the hydrolysis reaction. Hence, the nonprotonated merocyanine isomer is susceptible to hydrolysis, whereas the corresponding protonated form is stable toward hydrolytic degradation.

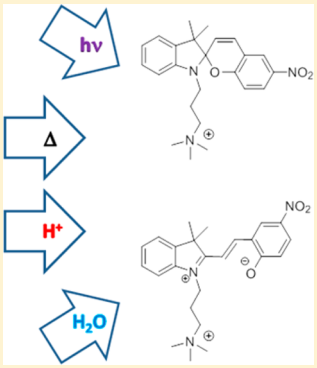

INTRODUCTION

Photochromic molecules from the spiropyran family are reversibly switched between the spiro form (SP), displaying absorption only in the UV region, and the merocyanine form (MC), absorbing light also in the visible region, using light of appropriate wavelengths.[1] Although the color change is the most widely recognized feature for spiropyrans and photoswitches in general, it is by no means the only property that changes upon isomerization. Additional examples are the redox energies,[2] molecular structure,[3] and charge distribution,[4] to mention a few. Altogether, the light-induced changes in these and other properties have been harnessed for applications in, for example, the photocontrol of biological functions,[5−13] bioimaging,[14−18] optical signal processing, and photoswitching in general,[19−30] as well as in chemosensing.[31−38] In many of these situations, aqueous media is required and, hence, also spiropyran derivatives that are readily dissolved in water. As the spiropyran backbone per se has very poor water solubility, covalent attachment of solubilizing groups, or supramolecular complex formation with water-soluble hosts have been used for this purpose.[5,29,39−45] Our approach has been to covalently attach positively charged alkylamino- or amidine groups to the spiropyran photoswitch. These compounds have been studied in the contexts of photo- and pH controlled DNA-binding,[5,7] photoinduced cytotoxicity,[9] membrane interactions,[8] and supramolecular complex formation.[44] Owing to the potential applicability in diverse fields, the ring-opening mechanism,[46−48] conformational distribution,[48,49] and photochemical properties[50,51] of various derivatives have also been addressed by theoretical investigations. Although the spiropyrans represent a very versatile class of photochromic compounds with several promising candidates for future use in biological applications, the behavior in aqueous media is relatively unexplored. Here, we present a comprehensive model of all processes relevant for the interconversions between the different species (SP, MC, and the respective protonated forms) including the thermal and photoinduced isomerization processes, as well as the undesired hydrolysis reaction. To support experiments, the hydrolytic degradation of the MC form was also investigated by theoretical calculations, using both quantum mechanics (QM) and combined quantum mechanics/molecular mechanics (QM/MM) models employing density functional theory. These addressed several mechanisms for both the protonated and the nonprotonated forms of the molecule and also the effect of water on the barrier heights, with final energies obtained at the B3LYP/6-311++G(2d,2p) level of theory. We hope that the results from this study will be of help to others in the design of spiropyran derivatives for various applications where aqueous media is a requirement.

EXPERIMENTAL SECTION

Materials. The synthesis of **1**,[5] **2**,[9] **4**,[44] and **6**[7] have been described earlier, whereas the synthesis of **3** and **5** are outlined in the Supporting Information. The ring-opened forms (MC and MCH^+) were prepared by heating the SP isomer in an aqueous solution at pH 1 until the sample was fully converted to the MCH^+ form (ca. 5 min). For MC, this was followed by neutralization of the pH using NaOH. The SPH^+ form was prepared by dissolving SP in aqueous solution followed by

Received: September 2, 2013
Revised: September 30, 2013
Published: October 21, 2013

Scheme 1. Interconversion Pathways between the Different Forms of the Spiropyran Derivatives, Here Exemplified for 1[a]

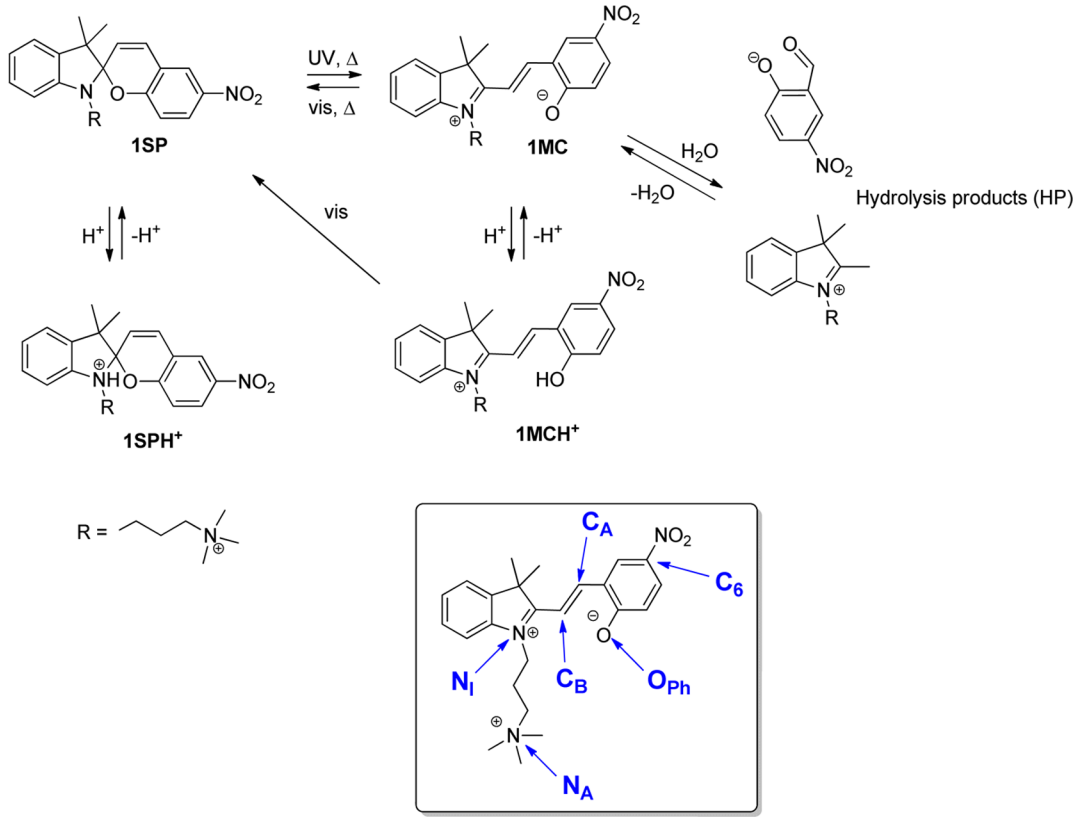

[a]Framed: Labelling of relevant atoms discussed in the text.

acidification with conc. HCl. Subsequent basification of the solution fully regenerated the SP form.

Photophysical Measurements. The absorption measurements were carried out on a CaryBio 50 UV/vis spectrometer equipped with a Varian PCB 1500 Water Peltier System thermostat for temperature control. Typically, the measurements were performed at 25 °C. The visible light was generated by a 500 W Xe lamp equipped with a hot mirror (A = 1.8 at 900 nm) to reduce the IR intensity and suitable optical filters. For quantum yield determinations, an interference filter in the visible region was used (see Supporting Information for details). The UV light was generated by a UVP lamp model UVGL-25 (254 nm, 700 μW/cm^2). The samples were continuously stirred during all irradiation processes.

The time-based absorption measurements at pH 4−10 were performed in buffered solutions with 10 mM Na_2HPO_4/NaH_2PO_4 set to the respective pH. At pH 3 and lower, the pH was set by adding standard portions of conc. HCl.

Computational Details. All quantum chemical calculations were performed using the Gaussian 09 software package.[52] To address the reaction mechanism of hydrolysis, two models were used. The reaction steps of the minimum energy path and the alternative reaction paths were addressed using a smaller QM model which included the initial merocyanine and one explicit water molecule (QM(1w)) (see Figure S6 in the Supporting Information). All the minima and transition states (TSs) for QM(1w) were optimized using Becke's three parameter hybrid functional[53] with the Lee−Yang−Parr correlation functional[54] (B3LYP) with the 6-31+G(d,p) basis set. This model considered solvent effects of water using the integral equation formalism for the polarizable continuum solvent model (IEFPCM).[55] To investigate potential effects of explicit water molecules on the barrier heights of the most important TSs, an ONIOM (our own N-layered integrated molecular orbital and molecular mechanics) integrated QM/MM method[56] model was used, in which six water molecules and the merocyanine were included in the QM layer, surrounded by a 40 Å box of explicit water molecules in a B3LYP/6-31G(d):AMBER setup (ONIOM(6w)). To ensure the relaxation of water equilibrated around MC, the final ONIOM(6w) model was obtained in several steps. Initially, the QM/MM model was fully minimized with only the MC molecule included in the QM layer. This was followed by an optimization with the water molecule closest to C_A (for labeling of atoms, see Scheme 1) included in the QM layer, and all water molecules farther than 15 Å from the MC molecule being frozen. Finally, five additional water molecules were chosen (the five closest to the C_A atom), resulting in three above and three below the plane of the merocyanine molecule (see Figure S6 in the Supporting Information). This way, the potential stabilizing contribution of water molecules from both sides of the MC molecule could be followed. For the QM layer atoms, charges were determined using the Merz−Singh−Kollman scheme[57] on the QM(1w) model, and for the remaining five water molecules the charges were determined after initial minimization.

The named TSs and minima were identified as for the QM(1w) model. Our focus was on the **MC** reactant state and on the three critical TSs, **TSI**, **TSII**, and **TSIII**, which were subject to further calculations.

All critical points obtained for QM(1w), and the above selected ones for ONIOM(6w), were followed by second derivative calculations at the same level of theory as

dx.doi.org/10.1021/jp408781p | J. Phys. Chem. B 2013, 117, 13561−13571

optimizations were performed. These were used to determine the nature of the optimized critical point (minimum or TS), to obtain both zero point energies and thermal contributions to the energy, and entropy contributions to free energies within the harmonic approximation.

In the case of QM(1w), for **III** and **TSIV** the initial reactant consists practically of two molecules coordinated only by one small group from each, which resulted in convergence problems with the molecular fragments rotating around the intermolecular axis. Therefore, convergence was achieved by constraining the relative orientation of the fragments for the above two critical points. This led to an additional imaginary vibrational frequency for both calculations, not related to the reaction coordinate. Due to the small magnitudes, $2i$ cm^{-1} and $12i$ cm^{-1}, respectively, the final energy values are not significantly affected. **TSIII** and the TS between the *TTT* and the *TTC* conformers of MCH$^+$ could not be located with the solvent model. Therefore, these two TSs were optimized at the same level of theory as the other critical points in the gas phase, followed by a single point calculation which considered solvent effects. For the two product states (**IV** and **HP**), the transformations between different coordination relative to each other were not considered. The transition state **HTSI** starting from the *TTC* conformer of MCH$^+$ was obtained using the loose convergence criteria as implemented in the Gaussian 09 software package.

Electronic energies were also calculated using point energy calculations at the B3LYP/6-311++G(2d,2p) and B3LYP/6-311++G(2d,2p):AMBER level of theory for QM(1w) and ONIOM(6w), respectively. For QM(1w) critical points **III**, **TSIV**, **IV**, and **HP** consist of two separate molecules coordinated to each other, why the single point energy calculations with higher basis set also serve the purpose of minimizing potential effects of basis set superposition errors observed with smaller basis sets.[58−60] For more details, see section "Theoretical Calculations" in the Supporting Information.

RESULTS AND DISCUSSION

The primary objective of this work has been to investigate in detail the various thermal, acido- and photochromic processes for the spiropyran derivatives shown in Figure 1. Compounds **1**−**4** have a nitro substituent in the 6-position of the benzopyran moiety (C_6, see Scheme 1 for labeling of relevant atoms discussed in the text). These compounds differ in the number of methylene units in the aminoalkyl-derived "tail" attached to the indoline nitrogen N_I (three or five), as well as the number of methyl groups on the amino nitrogen N_A (two or three). Compounds **5** and **6** are equipped with a quaternary amine via a propyl tail and come with an aldehyde and a cyano group on C_6, respectively. The main reason for using different substituents on the benzopyran ring was to vary the pK_a-value of the phenolic OH group of the protonated MC isomer (MCH$^+$, see Scheme 1).[61] A more electron withdrawing substituent is expected to stabilize the negatively charged oxygen O_{Ph} of the nonprotonated MC isomer and, hence, decrease the pK_a-value.[62] Moreover, the variation of the substituents at both the benzopyran ring and the indoline nitrogen N_I effects several other thermal and photoinduced processes, as will be described in detail below. In the following sections, the experimental results (spectra, kinetic traces, etc.) will be shown only for **1**, whereas the corresponding data for **2**−**6** is collected in the Supporting Information.

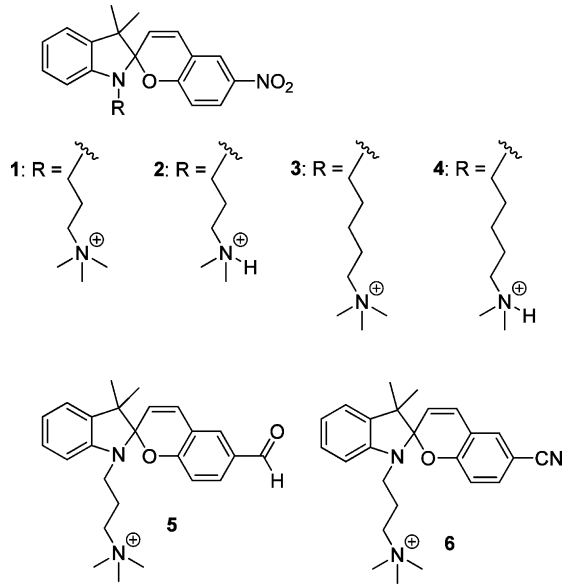

Figure 1. Structures of the closed spiro (SP) forms of the spiropyran derivatives studied in this work.

General Behavior. Scheme 1 shows the relevant forms of **1** and the corresponding interconversion pathways. The spectra of the respective forms are shown in Figure 2 (see Figure S1 in the Supporting Information for corresponding spectra of **2**−**6**).

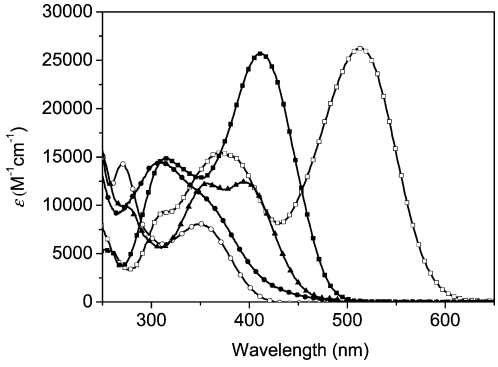

Figure 2. Absorption spectra of **1SP** (○), **1SPH**$^+$ (●), **1MC** (□), **1MCH**$^+$ (■), and HP (▲). At pH below ca. 4, HP displays absorbance only below 375 nm (not shown).

The SP isomer is converted to the MC isomer by UV-light exposure, and the reverse reaction is triggered by visible light. In the dark, the two isomers are interconverted by thermal processes. As opposed to organic solvents, where the thermal equilibrium is shifted to virtually 100% SP, the rate constants for the thermal isomerization processes SP → MC and MC → SP (k_o and k_c in Scheme 2) are comparable in aqueous solution. This is due to the highly polar nature of water which stabilizes the zwitterionic MC form. It has also been suggested that hydrogen bonding contributes to the MC form stabilization.[63]

Upon acidification, protonation of the MC phenolate oxygen O_{Ph} leads to the formation of MCH$^+$. Here, the pK_a-value of this form is referred to as pK_a^{II}. While this form is readily converted to SP using visible light, the corresponding thermal conversion is not observed. Moreover, we suggest that the MCH$^+$ isomer is stable also to hydrolytic degradation (*vide*

dx.doi.org/10.1021/jp408781p | J. Phys. Chem. B 2013, 117, 13561−13571

infra). Upon further acidification, also the SP isomer is protonated. We assign this species to SPH^+, where the indoline nitrogen N_I of the SP isomer is protonated, with a pK_a-value referred to herein as pK_a^I.[64] This form displays neither thermal nor photoinduced isomerizations, i.e., it can only be interconverted to the other forms after deprotonation to the SP isomer.[65] The pK_a-values of **1**−**6** are collected in Table 1. It

Table 1. pK_a-Values of SPH^+ (pKa^I) and MCH^+ (pKa^{II}) for 1−6

	1	2	3	4	5	6
pK_a^I	0.4	0.4	1.6	1.4	0.4	0.4
pK_a^{II}	3.7	4.2	4.4	4.2	4.5	4.4

is obvious that the substituent on C_6 influences pK_a^{II}, whereas it has no effect on pK_a^I.[61,66] The ability to tune the pK_a-value by the choice of substituent has been proven useful in many situations, including the pH-controlled DNA-binding observed in our laboratory.[7] Furthermore, pK_a^I for **1**−**6** are significantly lower compared to spiropyran derivatives without a positively charged functionality attached to the indoline nitrogen N_I. For example, pK_a^I of **1**, **2**, **5**, and **6** are almost two units lower compared to spiropyran derivatives with a methyl group attached to N_I (0.4 versus 2.3).[67] As SPH^+ cannot be converted to MC/MCH^+ by neither thermal nor photoinduced processes, this implies that the pH range over which **1**−**6** maintain their photochromic properties is significantly broadened.

Finally, one of the limiting factors for the application of spiropyrans in aqueous medium is the hydrolytic instability of the MC form.[45] Hydrolysis has been proposed to be initiated by nucleophilic attack at the ene-iminium cation, followed by a retro-aldol reaction yielding Fischer's base and salicylaldehyde as hydrolysis products (HP). Here, we suggest that the nonprotonated MC isomer is the only form that is susceptible to hydrolysis and that water is the major nucleophile involved in the reaction. Scheme 2 summarizes the kinetic model with the respective rate constants for the thermal processes and the pK_a-values for the protonated forms.

Scheme 2. Rate Constants for the Thermal Processes and pK_a-Values for the Protonated Forms SPH^+ and MCH^+

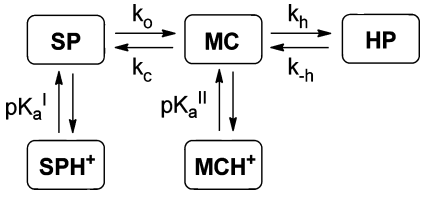

The sections below are organized as follows: First, the thermal processes (isomerization reactions and hydrolysis) at pH 7 will be described together with the photoinduced isomerization reactions. At pH 7, none of the protonated species are formed, i.e., the involved components are SP, MC, and HP. Second, the corresponding results at different pH will be presented for a selection of the derivatives. Our main objective in the design of **1**−**6** was to investigate the influence from the substituent on C_6 in the benzopyran ring. Hence, we concentrated on **1**, **5**, and **6** in this section.[61] The results from pH 5−9 suggest that water is the nucleophile in the hydrolysis reaction, rather than OH^-. In the pH-interval 0−1, the equilibrium MC/MCH^+ is shifted to nearly 100% MCH^+ and the hydrolysis reaction is virtually halted. Hence, our kinetic model in this pH range contains SPH^+, SP, and MCH^+. Based on these results, we suggest that MC is the only isomer that undergoes hydrolysis. Finally, we present computational results, which addressed the hydrolysis mechanism in aqueous media for both the MC and the MCH^+ forms that further strengthen the above notion.

Thermal and Photoinduced Processes at pH 7. Figure 3 shows the time-dependent absorbance of **1MC** reflecting the

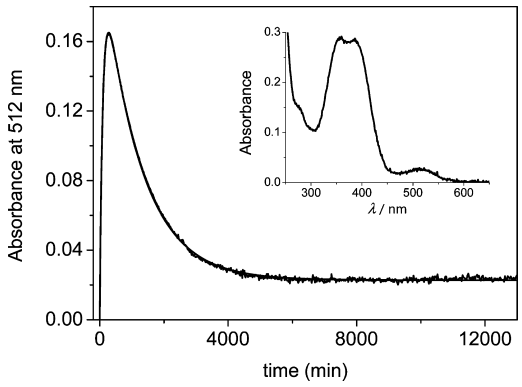

Figure 3. Kinetic absorption trace of **1MC** at 25 °C monitored at 512 nm reflecting the thermal interconversions between SP, MC, and HP according to eq 1. The solid line is the fitted trace using the biexponential expression in eq 2. Inset: Absorption spectrum recorded at t = 12000 min, clearly showing the residual absorption of **1MC** centered at 512 nm.

thermal interconversions of the dissolved SP and the MC forms together with the subsequent hydrolysis of MC. Similar kinetics with biexponential "rise and decay" behavior have been observed for other spiropyran derivatives.[40,45] As the pK_a-values of the SPH^+ and the MCH^+ forms of **1** were determined to 0.4 and 3.7, respectively, the concentrations of the protonated forms are negligible at pH 7 (see Table 1 for the pK_a-values of derivatives **1**−**6**). Hence, our kinetic model at this pH includes the species SP, MC, and HP. The absorbance of MC levels out at a nonzero value after ca. 8000 min, suggesting that the hydrolysis reaction is reversible.[68] Hence, the kinetic model shown in eq 1 was used to describe the kinetics at pH 7.

$$\mathrm{SP} \underset{k_c}{\overset{k_o}{\rightleftharpoons}} \mathrm{MC} \underset{k_{-h}}{\overset{k_h}{\rightleftharpoons}} \mathrm{HP} \tag{1}$$

This kinetic model gives rise to a biexponential rate expression for the concentrations of all involved species.[69] Thus, the kinetic trace was fitted according to eq 2.[70]

$$A = A_0 + ae^{-k_{rise}t} + be^{-k_{decay}t} \tag{2}$$

Here, k_{rise} reflects the rise time of the initial part of the kinetic trace in Figure 3, whereas k_{decay} is the rate constant of the subsequent decay. If $k_o + k_c \gg k_h + k_{-h}$, k_{rise} would have been the sum of k_o and k_c and, hence, the rise would reflect the rate of the thermal equilibrium establishment between SP and MC. Here, this assumption is not valid, and the analytic rate expressions for [SP], [MC], and [HP] derived using the Laplace transform method were used (see Supporting Information for the derived rate expressions).[69] The resulting rate constants for **1**−**6** are collected in Table 2.

It is obvious that there are large variations in both the ratio k_o/k_c as well as the sum $k_o + k_c$ between the different

dx.doi.org/10.1021/jp408781p | J. Phys. Chem. B 2013, 117, 13561−13571

Table 2. Rate Constants for the Thermal Processes, Isomerization Quantum Yields, and Photostationary Distribution (PSD) of compounds 1−6 at 25 °C at pH 7

	k_o [min^{-1}]	k_c [min^{-1}]	k_h [min^{-1}]	k_{-h} [min^{-1}]	k_o/k_c	Φ_o[a] %	Φ_c[b] %	PSD[c]
1	3.5×10^{-3}	5.1×10^{-3}	2.2×10^{-3}	9.8×10^{-5}	0.69	1.8	4.4	0.79
2	3.4×10^{-3}	3.9×10^{-3}	1.8×10^{-3}	~0	0.87	1.6	3.9	0.88
3	5.2×10^{-3}	1.4×10^{-3}	6.5×10^{-4}	1.9×10^{-5}	3.7	0.67	4.5	0.36
4	4.4×10^{-3}	1.5×10^{-3}	6.1×10^{-4}	1.1×10^{-5}	2.9	0.43	4.3	0.34
5	2.1×10^{-2}	5.0×10^{-2}	2.0×10^{-3}	1.2×10^{-4}	0.42	4.7	1.4	12
6	5.6×10^{-3}	3.4×10^{-2}	2.6×10^{-3}	5.4×10^{-5}	0.16	4.0	1.2	4.3

[a]Isomerization quantum yield for the process SP → MC using 254 nm UV-light. [b]Isomerization quantum yield for the process MC → SP using visible light centered at 503 nm. [c]Photostationary distribution [MC]/[SP] after the application of 254 nm UV-light.

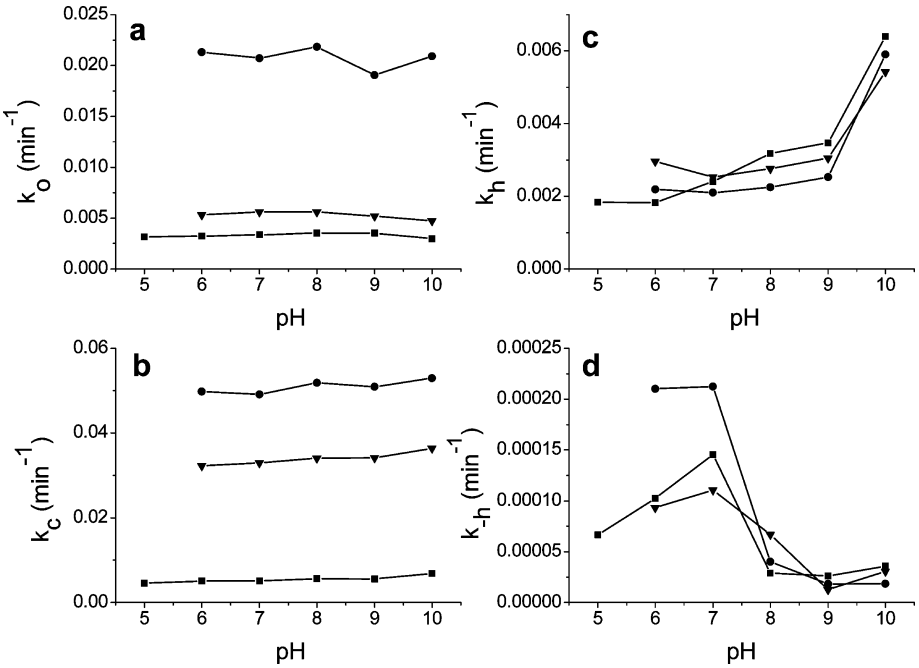

Figure 4. pH dependence of the thermal rate constants k_o (a), k_c (b), k_h (c), and k_{-h} (d). Data shown for **1** (■), **5** (●), and **6** (▼). The data is collected in Table S1 in the Supporting Information.

derivatives, which in turn manifest itself in differences in the hypothetical thermal equilibrium position [MC]/[SP] and the time required to reach it. For example, **3** contains ca. 80% MC at thermal equilibrium, whereas the corresponding number for **6** is only 14%. Depending on the application, both situations may be desired (visible-light activation to the SP form versus UV activation to the MC form). As for minimizing the effect of the hydrolytic degradation, a thermal equilibrium position enriched in SP is preferred, as the concentration of the hydrolyzable MC isomer is kept at a minimum. The quantum yields of the photoinduced isomerization processes and the photostationary distributions (PSD) are also collected in Table 1. The resistance toward photodegradation was controlled by exposing the samples to alternating UV/vis cycles. No detectable decomposition was observed after 10 cycles (see Figure S5 in the Supporting Information).

Thermal Processes at High pH. The experiments and the data analysis procedure at pH 7 described above were performed also at pH 5−10. Figure 4 shows the pH dependence of the rate constants k_o, k_c, k_h, and k_{-h} for **1**, **5**, and **6**. The extracted rate constants reflect the kinetic model shown in eq. 1, i.e., none of the protonated species SPH$^+$ or MCH$^+$ were considered. For **1**, this is a good approximation over the entire pH interval 5−10 as pK_a^{II} = 3.7 for this derivative, and hence, less than 5% exists as MCH$^+$ at pH 5. For **5** and **6**, the corresponding pK_a-values are 4.5 and 4.4. This implies that around 25% MCH$^+$ is present at pH 5, why the data is only shown between pH 6 and pH 10.

The rate constants for thermal opening and closing (k_o and k_c in Figure 4a,b) show no significant variations with pH. This is true also for the rate constant of hydrolysis MC → HP (k_h in Figure 4c) up to pH 9, whereas an increase by a factor of ca. 2 is observed at pH 10 for all derivatives. This strongly suggests that water is the major nucleophile in the hydrolysis reaction in the pH-independent interval up to pH 9, whereas the corresponding attack by OH$^-$ is the rate determining step at higher pH.[68] The data for the corresponding condensation reaction (reverse hydrolysis, k_{-h} in Figure 4d) shows that the process experiences a rate increase when going from pH 8 to pH 7. We will, however, not analyze the condensation reactions in the sections below, but instead focus on the hydrolysis reaction. The rate constants displayed in Figure 4 are tabulated in Table S1 in the Supporting Information.

Thermal Processes at Low pH. At pH significantly below pK_a^{II} (see Scheme 2 and Table 1) the MC/MCH$^+$ equilibrium is shifted to virtually only MCH$^+$. Hence, SP was dissolved at the respective pH and the rise in the absorbance of MCH$^+$ was

dx.doi.org/10.1021/jp408781p | J. Phys. Chem. B 2013, 117, 13561−13571

monitored as a function of time. The results for **1** at pH 0 and pH 1 are shown in Figure 5.

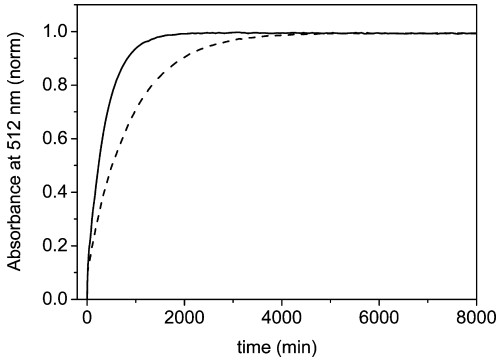

Figure 5. Thermal formation of **1MCH**$^+$ from **1SP** via **1MC** at pH 0 (dashed line) and pH 1 (solid line). The slower rise observed at pH 0 reflects the lower concentration of the thermally isomerizable SP form.

From the "rise and stay" behavior it is obvious that the hydrolysis reaction is virtually halted at pH 0 and pH 1. Therefore, the kinetic model in this pH regime is described by eq 3.

$$\mathrm{SPH^+} \overset{\mathrm{p}K_a^{\mathrm{I}}}{\rightleftharpoons} \mathrm{SP} \underset{k_c}{\overset{k_o}{\rightleftharpoons}} \mathrm{MC} \overset{\mathrm{p}K_a^{\mathrm{II}}}{\rightleftharpoons} \mathrm{MCH^+} \tag{3}$$

In this pH region, however, the [MC]/[MCH$^+$] equilibrium is shifted to virtually 100% MCH$^+$. Hence, the kinetic situation reduces to a model including only SPH$^+$, SP, and MCH$^+$ according to eq 4.

$$\mathrm{SPH^+} \overset{\mathrm{p}K_a^{\mathrm{I}}}{\rightleftharpoons} \mathrm{SP} \overset{k_o}{\rightarrow} \mathrm{MCH^+} \tag{4}$$

The kinetic traces were fitted to a monoexponential rate expression according to eq 5.

$$A = A_0(1 - ae^{-k_{\mathrm{rise}}t}) \tag{5}$$

The equilibrium establishment between SP and SPH$^+$ is extremely fast compared to k_o. Hence, the *apparent* rate constant of thermal opening, k_{rise}, is described by eq 6.

$$k_{\mathrm{rise}} = \frac{[\mathrm{SP}]}{[\mathrm{SP}] + [\mathrm{SPH^+}]} k_o \tag{6}$$

As pK_a for SPH$^+$ (pK_a^{I}, see Table 1) is known for all derivatives, the rate constant k_o is easily extracted from the experimentally fitted k_{rise}. The k_o-values at pH 0 and 1 were found to be: 4.0×10^{-3} min^{-1} and 3.4×10^{-3} min^{-1} for **1**, 1.3×10^{-2} min^{-1} and 2.0×10^{-2} min^{-1} for **5**, and 5.0×10^{-3} min^{-1} and 5.3×10^{-3} min^{-1} for **6**. These values agree very well with the corresponding values at pH 5 to pH 10 shown in Figure 4a. The fact that the rate constant of thermal opening SP → MC is virtually pH independent between pH 0 and 10 clearly shows that there is no direct accelerated acid induced opening SP → MCH$^+$, but that MCH$^+$ is formed via thermal opening SP → MC followed by protonation of MC.

Furthermore, no hydrolysis is seen over 8000 min at pH 0 and 1. If OH$^-$ would have been the nucleophile involved in the rate determining step, the halted hydrolysis could have been explained by the low OH$^-$ concentration at these pH values. This is highly unlikely, however, as the rate of hydrolysis does not vary significantly with the OH$^-$ concentration between pH 5 and 9. Thus, we suggest that MCH$^+$ is not susceptible to hydrolysis. This notion will be further supported by computational means (*vide infra*).

Thermal Processes at Intermediate pH. At pH 2−4, a full kinetic model including all species and processes shown in Scheme 2 has to be applied. We could not find the analytic expression for this kinetic situation by the Laplace transformation method. Instead we used the experimental rate constants derived at pH 5 and the respective pK_a-values to simulate the concentration profiles versus time for all relevant species by numerical means. These concentration profiles were compared with the experimentally recorded absorption traces of MC and MCH$^+$ at pH 2−4. While the experimentally obtained values of k_o and k_c at pH 5 together with pK_a^{I} and pK_a^{II} were used in the simulations, the values of k_h and k_{-h} were slightly adjusted for each pH-value to improve the goodness of fit (the experimental values at pH 5, $k_h = 1.8 \times 10^{-3}$ min^{-1}, $k_{-h} = 6.6 \times 10^{-5}$ min^{-1}, were varied in the intervals 1.8×10^{-3} min^{-1} − 2.6×10^{-3} min^{-1} and 0 − 6.6×10^{-5} min^{-1}, respectively). Note that these adjustments are no larger than the variations in the experimentally obtained values of k_h and k_{-h} between pH 5 and pH 10. The results for **1** are shown in Figure 6 and the corresponding data for **5** and **6** is shown in Figure S4 in the Supporting Information. The results clearly show that the kinetic model holds also at pH values where the interconversions between all five species have to be taken into account.

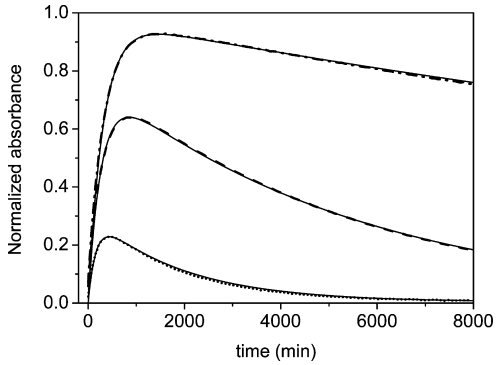

Figure 6. Experimentally recorded absorbance traces for **1MC** and **1MCH**$^+$ at 25 °C at pH 2 (dash-dot, recorded at 410 nm, MCH$^+$), pH 3 (dashed, recorded at 410 nm, MC and MCH$^+$), and pH 4 (dotted, recorded at 512 nm, MC). The corresponding normalized traces derived from a simulation using the kinetic model in Scheme 2 and the rate constants at pH 5 are also shown (solid lines). Note that k_h and k_{-h} were slightly adjusted from the values determined at pH 5 (see text for details).

Theoretical Investigation of Hydrolysis. To support experiments, the mechanism of hydrolysis of the MC isomer was investigated in detail by theoretical calculations. The reaction steps were explored using a QM model with one explicit water molecule considered, referred to herein as QM(1w), whereas the effect of solvent molecules on the barrier height was also addressed with a larger ONIOM model.[56] Here, six water molecules were included in the QM layer, further surrounded by water molecules treated by MM (ONIOM(6w)). Fortunately, in recent years several theoretical studies have focused on various spectral properties of the SP ⇄ MC conversion mechanism of spiropyrans and related derivatives, which greatly helped in selecting the optimal models and the applied theoretical method.[46,47,49−51] Balasu-

dx.doi.org/10.1021/jp408781p | J. Phys. Chem. B 2013, 117, 13561−13571

bramanian et al. have analyzed in detail the effect of several density functionals and continuum solvent models on relative energies of different conformers.[49] Based on these results and on previous tests on hydrolysis reactions using Møller−Plesset (MP2) calculations as a reference,[71,72] geometry optimizations for the QM(1w) model were performed at the B3LYP/6-31+G(d,p) level of theory with solvent effects of water considered by the IEFPCM model.[73] Final energies were obtained from point energy calculations at the B3LYP/6-311++G(2d,2p) level. All energetic values are discussed at the latter level unless noted otherwise.

Prior to addressing the reaction steps, the initial "reactant" conformer of MC was selected based on considering the four different relative orientations of the *p*-nitro-phenolate and the indolenium groups. Based on previous results[48] and on our analysis (see Supporting Information), we concluded that the *TTC* conformer is the major initial reactant and, hence, was used in the calculations. The initial *TTC* conformer was optimized with four alternative water positions close to C_A and the lowest energy conformer was selected to be the reactant state (**MC**) as shown in Figure 7. A similar analysis was

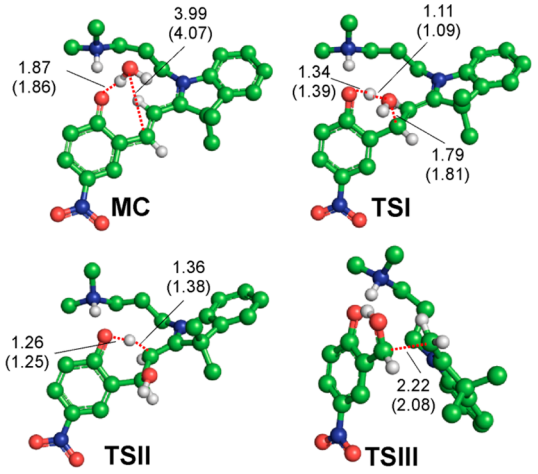

Figure 7. Selected critical points along the minimum energy path starting from the *TTC* conformer with the nucleophilic water molecule coordinated on the molecule (**MC**). The obtained critical points were qualitatively the same for the QM(1w) and ONIOM(6w) models. Relevant distances of the atoms participating in the hydrolysis are displayed for the QM(1w) and in parentheses for the ONIOM(6w) with values in Ångströms. For more details, see Tables 3 and 4, and Figures S6 and S7 in the Supporting Information.

performed for the protonated form, MCH^+, where the energetic distribution of the conformers showed that the *TTT* conformer is somewhat more stable than the *TTC* conformer. However, the two conformers are separated by only a low energy transition state (TS) as detailed in the Supporting Information, why we addressed the reaction paths starting from both *TTC* and *TTT* conformers for MCH^+.

To determine the most likely minimum energy pathway of the reaction, several alternative mechanisms were initially considered using QM(1w). These include two different paths starting from the neutral form, MC, and also two paths starting from the protonated form, MCH^+. The energy profile of the reaction was compared with the free energy values derived back from the experimental rate constants of hydrolysis shown in Table 2 using classical transition state theory.[74] Out of the reaction pathways mentioned above, those which resulted in unlikely high energy values for TSs or for intermediate structures were excluded from further analysis. For more details on the calculations, see the Experimental Section, and "Theoretical Calculations" in the Supporting Information.

The MC Form. The structure of the hydrolysis products shows that the nucleophilic attack of the water molecule takes place on the double-bond between the nitro-phenolate and the indolenium fragments, with the water oxygen (O^W) coupling to carbon atom C_A (for labeling of the atoms see Scheme 1 and Scheme 3). Accordingly, in the initial reactant state **MC**, for

Scheme 3. The Mechanism of Hydrolysis for MC along the Minimum Energy Pathway As Determined by the QM Calculations[a]

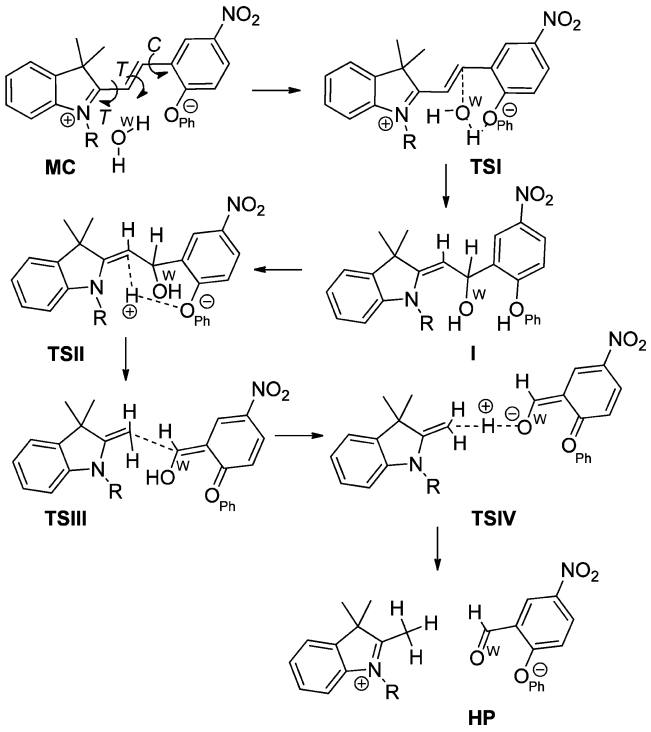

[a]Only selected critical points required to clearly show the reaction mechanism are displayed. For all reaction steps, see Figure S7 in the Supporting Information. The nomenclature of the different conformers in the reactant state **MC** is based on the *cis* or *trans* position of the central three bonds, here shown for the lowest energy conformer, *TTC*.

both QM(1w) and ONIOM(6w) models, the water molecule is coordinated on the phenolate oxygen O_{Ph} close to the central C_A-C_B double bond as shown in Figure 7 and Figure S7 in the Supporting Information. The reaction in QM(1w) then proceeds via the first transition state (**TSI**) with a barrier of 26.5 kcal/mol into the first intermediate (**I**), in which O_{Ph} becomes protonated and the OH group from the water molecule (O^W-H) forms a bond with C_A. Judging from the structure of the hydrolysis products, the protons from the two OH groups eventually have to transfer to the opposite carbon, C_B, which will finally result in a methyl group on the indolenium fragment. From intermediate **I**, the overall reaction could in principle proceed with a double proton transfer, where O^W-H protonates C_B, together with simultaneous O^W protonation by $O_{Ph}-H$ (see Scheme 3). However, the corresponding TS energy shown in Figure 8 is above 40

dx.doi.org/10.1021/jp408781p | J. Phys. Chem. B 2013, 117, 13561−13571

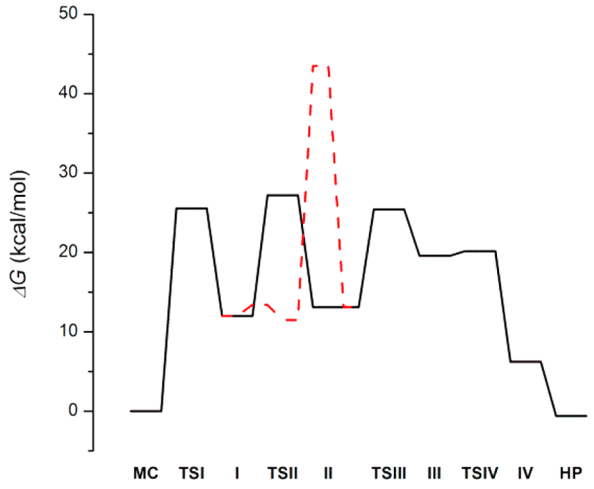

Figure 8. Reaction profile for hydrolysis of the MC isomer obtained using the QM(1w) model. Energy values for the minimum energy pathway via the phenolate mediated proton transfer (solid line), and the reaction pathway with direct protonation (dashed line) were obtained considering solvent effects of water at the IEFPCM-B3LYP/6-31+G(d,p) level of theory.

kcal/mol, which renders this reaction path very unlikely. Instead, the structure of intermediate **I** allows for a direct protonation of C_B from O_{Ph}–H, with a barrier height of 28.9 kcal/mol at **TSII** (see Table 3 and Figures 7 and 8). From this

Table 3. Energetic Properties of the Reaction Steps for MC along the Minimum Energy Pathway Obtained Using the QM(1w) Model at Different Levels of Theory

	B3LYP/6-31+G(d,p)[a]			B3LYP/6-311++G(2d,2p)[b]		
step	ΔE[c]	ΔH	ΔG	ΔE	ΔH	ΔG
MC	0.0	0.0	0.0	0.0	0.0	0.0
TSI	23.8	21.6	25.5	24.7	22.5	26.5
I	9.0	10.3	12.0	9.3	10.6	12.3
TSII	24.8	22.7	27.2	26.5	24.4	28.9
II	9.7	11.1	13.1	11.2	12.6	14.6
TSIII[d]	23.1	21.7	25.4	24.0	22.5	26.2
III	23.2	22.5	19.6	23.8	22.4	19.4
TSIV	24.7	21.3	20.2	25.2	21.8	20.7
IV	6.9	6.3	6.2	7.8	7.2	7.1
HP	0.8	−0.5	−0.6	1.8	0.4	0.3

[a]Using IEFPCM solvent model for water. [b]Using the IEFPCM-B3LYP/6-31+G(d, p) structure and IEFPCM solvent model for water. [c]Values are in kcal/mol. [d]**TSIII** structure was obtained in the gas phase at the B3LYP/6-31+G(d,p) level of theory.

point, intermediate **II**, the reaction proceeds with the breakup of the bond between C_A and C_B via **TSIII**, with ΔG = 26.5 kcal/mol. In intermediate **III** the fragments are coordinated with O^W–H on C_B, which is in sp^2 hybridization. Although at this point the proton is still bonded to the oxygen, the extended conjugation with the ring system renders the molecule in a planar conformation. Finally the protonation of C_B takes place with a small barrier from **III** (19.4 kcal/mol) through **TSIV** (20.7 kcal/mol), and the hydrolysis products are formed (**IV** and **HP**). Considering reaction energetics of the minimum energy path, there are three TSs: **TSI**, **TSII**, and **TSIII**, which have similar relative energies where the highest barrier corresponds to the transfer of the first proton to C_B from O_{Ph} (**TSII**) with a free energy of 27.2 and 28.9 kcal/mol at the B3LYP/6-31+G(d,p) and B3LYP/6-311++G(2d,2p) levels of theory, respectively. Considering the reactant and the product states, **MC** and **HP**, the small relative energy difference, −0.6 and 0.3 kcal/mol for the B3LYP/6-31+G(d,p) and B3LYP/6-311++G(2d,2p) levels, respectively, are in line with the ratios of k_h and k_{-h} displayed in Table 2. This is also in accordance with other similar hydrolysis reactions, where reversibility was observed.[68] Note that after the breakup of the C_A–C_B bond at **TSIII**, there are two molecular fragments, and the following steps in the reaction involve a shallow TS in our investigation. Consequently, the formation of the final two hydrolysis product molecules could in principle also be achieved by proton transfers with other solvent molecules that the present quantum chemical calculations do not consider.

To address the effects of further explicit water molecules on the barrier height with a different approach, the initial MC form and the three high energy TSs were also investigated in the ONIOM(6w) model. Despite major differences in the QM(1w) and ONIOM(6w) models, the main structural parameters of the optimized **MC**, **TSI** and **TSII** critical points are very similar as seen in Figure 7. The largest difference can be observed for **TSIII**, where the distance between C_A and C_B is 2.22 Å and 2.08 Å for the QM(1w) and ONIOM(6w) models, respectively.

In terms of energetics, the ONIOM(6w) free energy barrier heights are all lower than the values for the corresponding TSs in QM(1w). When the ΔE values presented in Table 4 are

Table 4. TS Barrier Heights Obtained for the QM(1w) Model and the ONIOM(6w) Model Using the MC Critical Point as Reference

	QM(1w)[a]			ONIOM(6w)[b]		
step	ΔE[c]	ΔH	ΔG	ΔE	ΔH	ΔG
TSI	24.7	22.5	26.5	23.6	19.3	18.9
TSII	26.5	24.4	28.9	23.9	21.9	24.0
TSIII	24.0	22.5	26.2	13.3	11.4	7.4

[a]The relative energies were obtained at the IEFPCM-B3LYP/6-311++G(2d,2p)//IEFPCM-B3LYP/6-31+G(d,p) level of theory. [b]The relative energies were obtained with B3LYP/6-311++G(2d,2p):AMBER setup calculated on B3LYP/6-31G(d):AMBER structures. [c]All values are in kcal/mol.

compared for **TSI** and **TSII**, it is seen that they are similar for the two models. Thus, the lower free energies arise from the more favorable relative entropy terms and also from some smaller extra stabilization by the surrounding water molecules. However, in the case of **TSIII** the final energies are significantly lower for the ONIOM(6w) than for the QM(1w) model. To understand the underlying reasons for this difference, we have analyzed the components of the ONIOM energies, which is briefly discussed here. The electronic relative energy of only the QM layer is 31.3 kcal/mol for **TSIII** at the B3LYP/6-311++G(2d,2p) level, which is 18.6 kcal/mol from the total ONIOM ΔE of 13.3 kcal/mol obtained with the B3LYP/6-311++G(2d,2p):AMBER setup shown in Table 4. This clearly shows that the different **TSIII** geometry with 2.08 Å $C_A \cdots C_B$ distance in the ONIOM(6w) compared to the 2.22 Å as obtained for the QM(1w) has no substantial effect on the barrier height. The excess stabilization of **TSIII** in the ONIOM(6w) model is rather caused by the favorable contributions of the water molecules in the MM layer: the

dx.doi.org/10.1021/jp408781p | J. Phys. Chem. B 2013, 117, 13561−13571

Coulomb and the van der Waals terms are, respectively, 9.8 and 8.7 kcal/mol more favorable in **TSIII** compared to **MC**.

In overall, the major difference arising from considering explicit water molecules is that for the QM(1w) model there are three high energy TSs, while for the ONIOM(6w) model there is only one TS found with higher energy: **TSII**. For both models this is the highest TS with a 28.9 and 24.0 kcal/mol barrier height for the QM(1w) and ONIOM(6w) models, respectively. Although further refinement of the energy values, e.g., by investigating several QM/MM water configurations or by obtaining conformational entropy contributions using MD sampling is beyond our scope, the obtained values can be used for a qualitative comparison with the experimental rates. Free energy values can be derived back from the experimental rate constants k_h displayed in Table 2 using classical transition state theory. These are ∼23−24 kcal/mol, which is in close agreement with the theoretical values.

The MCH$^+$ Form. To consider further paths for hydrolysis, we have also investigated the protonated form MCH$^+$ using the QM(1w) model starting from both of its two lowest energy conformers, *TTC* and *TTT* (See Figure S8, Table S2 and text in the Supporting Information). In the reactant form, referred to as **MCH$^+$**, the O_{Ph}−H group is clearly less prone to accept a proton from the nucleophilic water molecule. To test this reaction path, we have obtained in principle the protonated form of the first intermediate, **HI$_{alt}$** (see Figure S8 in the Supporting Information). Here O_{Ph}−H accepts an additional H^+, resulting in the formation of O_{Ph}−H_2^+, and the remaining OH^- from the water molecule forms a bond with C_A. The relative energy of this intermediate is very high, 58.4 kcal/mol for *TTC*, and for *TTT* we could not even locate this critical point as calculations converged back to the reactant state. In an alternative pathway, the reaction could start with the addition of water directly to the central C_A−C_B double-bond, with OH^- forming a bond with C_A, and H^+ coupling to C_B. However, this reaction path is also much higher than any critical point along the reaction observed for MC, as the corresponding TS has a relative energy of 49.9 and 48.5 kcal/mol for the *TTC* and *TTT* conformers, respectively. The very high energy critical points observed for the hydrolysis paths of MCH$^+$ are clearly a consequence of either the protonation *per se*, or the fact that a direct addition of water to the central C_A−C_B double bond is unfavorable. The similarity of the results obtained for *TTC* and *TTT* demonstrates that a change in the initial MCH$^+$ conformation for this reaction would not alter the energetics significantly. Furthermore, considering the structure of the hydrolysis products HP, the initial addition of water cannot take place in any alternative way, which is why we conclude that MCH$^+$ is not susceptible to hydrolysis.

CONCLUSIONS

We have investigated the behavior of six spiropyran derivatives in aqueous solution between pH 0 and 10. The following conclusions can be drawn: (*i*) The substitution pattern influences substantially the rates of the thermal isomerization processes as well as the pK_a-values for the protonated forms of SP and MC (SPH$^+$ and MCH$^+$). Interestingly, the pK_a of SPH$^+$ is decreased by as much as ∼2 units by the attachment of positively charged amino groups to the indoline nitrogen via alkyl linkers. This allows for photoinduced isomerizations between the SP and the MC forms over a wider pH range. (*ii*) The *apparent* rate of hydrolysis of the MC isomer varies significantly with the substitution pattern. This, however, is a result of the differences in the thermal equilibrium positions [MC]/[SP], whereas the intrinsic rate constant of hydrolysis is virtually the same for all derivatives. (*iii*) The rate constant of hydrolysis does not vary significantly between pH 5 and 9, clearly suggesting that water is the nucleophile in this pH range. (*iv*) The nonprotonated MC isomer is the only form that is susceptible to hydrolysis. This is due to the key role of the phenolate oxygen, acting as a base by accepting a proton from the nucleophilic water, and later transferring it to the farther carbon, C_B. As a consequence, the hydrolytic degradation is halted at pH values where MCH$^+$ is the dominating open form.

ASSOCIATED CONTENT

Supporting Information

Synthetic procedures, determination of isomerization quantum yields, details on the Laplace transformation analysis, spectroscopic data for selected derivatives, photocycling experiments, details on theoretical methods, applied theoretical models, and critical points obtained for MC and MCH$^+$ forms. This information is available free of charge via the Internet at http://pubs.acs.org.

AUTHOR INFORMATION

Corresponding Author

*E-mail: a-son@chalmers.se; Tel: +46 31 772 28 38; Fax: +46 31 772 38 58.

Notes

The authors declare no competing financial interest.

ACKNOWLEDGMENTS

This work was financed by the Swedish Research Council (Grant 622-2010-280) and the European Research Council (ERC FP7/2007-2013 Grant No. 203952).

REFERENCES

(1) Bouas-Laurent, H.; Dürr, H. Organic photochromism. *Pure Appl. Chem.* **2001**, *73*, 639−665.

(2) Terazono, Y.; Kodis, G.; Andréasson, J.; Jeong, G.; Brune, A.; Hartmann, T.; Dürr, H.; Moore, A. L.; Moore, T. A.; Gust, D. Photonic Control of Photoinduced Electron Transfer via Switching of Redox Potentials in a Photochromic Moiety. *J. Phys. Chem. B* **2004**, *108*, 1812−1814.

(3) Vomasta, D.; Högner, C.; Branda, N. R.; König, B. Regulation of Human Carbonic Anhydrase I (hCAI) Activity by Using a Photochromic Inhibitor. *Angew. Chem., Int. Ed.* **2008**, *47*, 7644−7647.

(4) Andréasson, J.; Terazono, Y.; Albinsson, B.; Moore, T. A.; Moore, A. L.; Gust, D. Molecular AND Logic Gate Based on Electric Dichroism of a Photochromic Dihydroindolizine. *Angew. Chem., Int. Ed.* **2005**, *44*, 7591−7594.

(5) Andersson, J.; Li, S. M.; Lincoln, P.; Andréasson, J. Photoswitched DNA-Binding of a Photochromic Spiropyran. *J. Am. Chem. Soc.* **2008**, *130*, 11836−11837.

(6) Beyer, C.; Wagenknecht, H. A. Synthesis of DNA with Spirobenzopyran as an Internal Covalent Modification. *Synlett* **2010**, 1371−1376.

(7) Hammarson, M.; Andersson, J.; Li, S. M.; Lincoln, P.; Andréasson, J. Molecular AND-Logic for Dually Controlled Activation of a DNA-Binding Spiropyran. *Chem. Commun.* **2010**, *46*, 7130−7132.

(8) Jonsson, F.; Beke-Somfai, T.; Andréasson, J.; Nordén, B. Interactions of a Photochromic Spiropyran with Liposome Model Membranes. *Langmuir* **2013**, *29*, 2099−2103.

(9) Nilsson, J. R.; Li, S. M.; Önfelt, B.; Andréasson, J. Light-Induced Cytotoxicity of a Photochromic Spiropyran. *Chem. Commun.* **2011**, *47*, 11020−11022.

(10) Sakata, T.; Yan, Y. L.; Marriott, G. Optical Switching of Dipolar Interactions on Proteins. *Proc. Natl. Acad. Sci. U.S.A.* **2005**, *102*, 4759−4764.
(11) Sunamoto, J.; Iwamoto, K.; Mohri, Y.; Kominato, T. Liposomal membranes 0.13. Transport of an Amino-Acid Across Liposomal Bilayers as Mediated by a Photoresponsive Carrier. *J. Am. Chem. Soc.* **1982**, *104*, 5502−5504.
(12) Tong, R.; Hemmati, H. D.; Langer, R.; Kohane, D. S. Photoswitchable Nanoparticles for Triggered Tissue Penetration and Drug Delivery. *J. Am. Chem. Soc.* **2012**, *134*, 8848−8855.
(13) Young, D. D.; Deiters, A. Light-Regulated RNA-Small Molecule Interactions. *ChemBioChem* **2008**, *9*, 1225−1228.
(14) Mao, S.; Benninger, R. K. P.; Yan, Y. L.; Petchprayoon, C.; Jackson, D.; Easley, C. J.; Piston, D. W.; Marriott, G. Optical Lock-in Detection of FRET Using Synthetic and Genetically Encoded Optical Switches. *Biophys. J.* **2008**, *94*, 4515−4524.
(15) Marriott, G.; Mao, S.; Sakata, T.; Ran, J.; Jackson, D. K.; Petchprayoon, C.; Gomez, T. J.; Warp, E.; Tulyathan, O.; Aaron, H. L.; Isacoff, E. Y.; Yan, Y. L. Optical Lock-in Detection Imaging Microscopy for Contrast-Enhanced Imaging in Living Cells. *Proc. Natl. Acad. Sci. U.S.A.* **2008**, *105*, 17789−17794.
(16) Tian, Z. Y.; Wu, W. W.; Wan, W.; Li, A. D. Q. Single-Chromophore-Based Photoswitchable Nanoparticles Enable Dual-Alternating-Color Fluorescence for Unambiguous Live Cell Imaging. *J. Am. Chem. Soc.* **2009**, *131*, 4245−4252.
(17) Zhu, L. Y.; Wu, W. W.; Zhu, M. Q.; Han, J. J.; Hurst, J. K.; Li, A. D. Q. Reversibly Photoswitchable Dual-Color Fluorescent Nanoparticles as New Tools for Live-Lell Imaging. *J. Am. Chem. Soc.* **2007**, *129*, 3524−3526.
(18) Zhu, M. Q.; Zhang, G. F.; Li, C.; Aldred, M. P.; Chang, E.; Drezek, R. A.; Li, A. D. Q. Reversible Two-Photon Photoswitching and Two-Photon Imaging of Immunofunctionalized Nanoparticles Targeted to Cancer Cells. *J. Am. Chem. Soc.* **2011**, *133*, 365−372.
(19) Andréasson, J.; Straight, S. D.; Kodis, G.; Park, C. D.; Hambourger, M.; Gervaldo, M.; Albinsson, B.; Moore, T. A.; Moore, A. L.; Gust, D. All-Photonic Molecular Half-Adder. *J. Am. Chem. Soc.* **2006**, *128*, 16259−16265.
(20) Bahr, J. L.; Kodis, G.; de la Garza, L.; Lin, S.; Moore, A. L.; Moore, T. A.; Gust, D. Photoswitched Singlet Energy Transfer in a Porphyrin−Spiropyran Dyad. *J. Am. Chem. Soc.* **2001**, *123*, 7124−7133.
(21) Garcia, A. A.; Cherian, S.; Park, J.; Gust, D.; Jahnke, F.; Rosario, R. Photon-Controlled Phase Partitioning of Spiropyrans. *J. Phys. Chem. A* **2000**, *104*, 6103−6107.
(22) Guo, X. F.; Zhang, D. Q.; Zhang, G. X.; Zhu, D. B. Monomolecular Logic: "Half-Adder" Based on Multistate/Multifunctional Photochromic Spiropyrans. *J. Phys. Chem. B* **2004**, *108*, 11942−11945.
(23) Natali, M.; Giordani, S. Molecular Switches as Photocontrollable "Smart" Receptors. *Chem. Soc. Rev.* **2012**, *41*, 4010−4029.
(24) Raymo, F. M.; Giordani, S. Signal Processing at the Molecular Level. *J. Am. Chem. Soc.* **2001**, *123*, 4651−4652.
(25) Raymo, F. M.; Giordani, S. All-Optical Processing With Molecular Switches. *Proc. Natl. Acad. Sci. U.S.A.* **2002**, *99*, 4941−4944.
(26) Remón, P.; Hammarson, M.; Li, S. M.; Kahnt, A.; Pischel, U.; Andréasson, J. Molecular Implementation of Sequential and Reversible Logic Through Photochromic Energy Transfer Switching. *Chem.—Eur. J.* **2011**, *17*, 6492−6500.
(27) Silvi, S.; Arduini, A.; Pochini, A.; Secchi, A.; Tomasulo, M.; Raymo, F. M.; Baroncini, M.; Credi, A. A Simple Molecular Machine Operated by Photoinduced Proton Transfer. *J. Am. Chem. Soc.* **2007**, *129*, 13378−13379.
(28) Silvi, S.; Constable, E. C.; Housecroft, C. E.; Beves, J. E.; Dunphy, E. L.; Tomasulo, M.; Raymo, F. M.; Credi, A. All-Optical Integrated Logic Operations Based on Chemical Communication between Molecular Switches. *Chem.—Eur. J.* **2009**, *15*, 178−185.
(29) Tomizaki, K. Y.; Mihara, H. Phosphate-Mediated Molecular Memory Driven by Two Different Protein Kinases as Information Input Elements. *J. Am. Chem. Soc.* **2007**, *129*, 8345−8352.
(30) Yildiz, I.; Impellizzeri, S.; Deniz, E.; McCaughan, B.; Callan, J. F.; Raymo, F. M. Supramolecular Strategies To Construct Biocompatible and Photoswitchable Fluorescent Assemblies. *J. Am. Chem. Soc.* **2011**, *133*, 871−879.
(31) Darwish, T. A.; Evans, R. A.; James, M.; Hanley, T. L. Spiropyran-Amidine: A Molecular Canary for Visual Detection of Carbon Dioxide Gas. *Chem.—Eur. J.* **2011**, *17*, 11399−11404.
(32) Fries, K.; Samanta, S.; Orski, S.; Locklin, J. Reversible Colorimetric Ion Sensors Based on Surface Initiated Polymerization of Photochromic Polymers. *Chem. Commun.* **2008**, 6288−6290.
(33) Han, S. L.; Chen, Y. Colorimetric Probing of Hg^{2+} in Both Solution and Thin Film. *Anal. Methods* **2011**, *3*, 557−559.
(34) Natali, M.; Soldi, L.; Giordani, S. A Photoswitchable Zn (II) Selective Spiropyran-Based Sensor. *Tetrahedron* **2010**, *66*, 7612−7617.
(35) Sakata, T.; Jackson, D. K.; Mao, S.; Marriott, G. Optically Switchable Chelates: Optical Control and Sensing of Metal Ions. *J. Org. Chem.* **2008**, *73*, 227−233.
(36) Shao, N.; Jin, J. Y.; Cheung, S. M.; Yang, R. H.; Chan, W. H.; Mo, T. A Spiropyran-Based Ensemble for Visual Recognition and Quantification of Cysteine and Homocysteine at Physiological Levels. *Angew. Chem., Int. Ed.* **2006**, *45*, 4944−4948.
(37) Shao, N.; Jin, J. Y.; Wang, H.; Zheng, J.; Yang, R. H.; Chan, W. H.; Abliz, Z. Design of Bis-spiropyran Ligands as Dipolar Molecule Receptors and Application to in Vivo Glutathione Fluorescent Probes. *J. Am. Chem. Soc.* **2010**, *132*, 725−736.
(38) Wohl, C. J.; Helms, M. A.; Chung, J. O.; Kuciauskas, D. Phospholipid Bilayer Free Volume Analysis Employing the Thermal Ring-Closing Reaction of Merocyanine Molecular Switches. *J. Phys. Chem. B* **2006**, *110*, 22796−22803.
(39) Kohl-Landgraf, J.; Braun, M.; Özcoban, C.; Goncalves, D. P. N.; Heckel, A.; Wachtveietl, J. Ultrafast Dynamics of a Spiropyran in Water. *J. Am. Chem. Soc.* **2012**, *134*, 14070−14077.
(40) Li, R.; Santos, C. S.; Norsten, T. B.; Morimitsu, K.; Bohne, C. Aqueous Solubilization of Photochromic Compounds by Bile Salt Aggregates. *Chem. Commun.* **2010**, *46*, 1941−1943.
(41) Miskolczy, Z.; Biczók, L. Photochromism in Cucurbit[8]uril Cavity: Inhibition of Hydrolysis and Modification of the Rate of Merocyanine−Spiropyran Transformations. *J. Phys. Chem. B* **2011**, *115*, 12577−12583.
(42) Miskolczy, Z.; Biczók, L. Selective Acceleration of the Protonated Merocyanine−Spiropyran Photochromic Transformation by Inclusion in Cucurbit[7]uril. *Photochem. Photobiol.* **2012**, *88*, 1461−1466.
(43) Miskolczy, Z.; Biczók, L. Photochromism of a Merocyanine Dye Bound to Sulfonatocalixarenes: Effect of pH and the Size of Macrocycle on the Kinetics. *J. Phys. Chem. B* **2013**, *117*, 648−653.
(44) Nilsson, J. R.; Carvalho, C. P.; Li, S. M.; Da Silva, J. P.; Andréasson, J.; Pischel, U. Switching Properties of a Spiropyran-Cucurbit[7]uril Supramolecular Assembly: Usefulness of the Anchor Approach. *ChemPhysChem* **2012**, *13*, 3691−3699.
(45) Stafforst, T.; Hilvert, D. Kinetic Characterization of Spiropyrans In Aqueous Media. *Chem. Commun.* **2009**, 287−288.
(46) Castro, P. J.; Gomez, I.; Cossi, M.; Reguerot, M. Computational Study of the Mechanism of the Photochemical and Thermal Ring-Opening/Closure Reactions and Solvent Dependence in Spirooxazines. *J. Phys. Chem. A* **2012**, *116*, 8148−8158.
(47) Ganesan, R.; Remacle, F. Stabilization of Merocyanine by Protonation, Charge, and External Electric Fields and Effects on the Isomerization of Spiropyran: A Computational Study. *Theor. Chem. Acc.* **2012**, *131*, 1255.
(48) Sheng, Y. H.; Leszczynski, J.; Garcia, A. A.; Rosario, R.; Gust, D.; Springer, J. Comprehensive Theoretical Study of the Conversion Reactions of Spiropyrans: Substituent and Solvent Effects. *J. Phys. Chem. B* **2004**, *108*, 16233−16243.
(49) Balasubramanian, G.; Schulte, J.; Müller-Plathe, F.; Böhm, M. C. Structural and Thermochemical Properties of a Photoresponsive Spiropyran and Merocyanine Pair: Basis Set and Solvent Dependence in Density Functional Predictions. *Chem. Phys. Lett.* **2012**, *554*, 60−66.

(50) Kumar, S.; Velasco, K.; McCurdy, A. X-ray, Kinetics and DFT Studies of Photochromic Substituted Benzothiazolinic Spiropyrans. *J. Mol. Struct.* **2010**, *968*, 13−18.
(51) Murugan, N. A.; Chakrabarti, S.; Ågren, H. Solvent Dependence of Structure, Charge Distribution, and Absorption Spectrum in the Photochromic Merocyanine-Spiropyran Pair. *J. Phys. Chem. B* **2011**, *115*, 4025−4032.
(52) Frisch, M. J. et al. *Gaussian 09*, revision A.1; Gaussian, Inc., Wallingford, CT, 2009.
(53) Becke, A. D. A New Mixing of Hartree-Fock and Local Density-Functional Theories. *J. Chem. Phys.* **1993**, *98*, 1372−1377.
(54) Lee, C. T.; Yang, W. T.; Parr, R. G. Development of the Colle−Salvetti Correlation-Energy Formula into a Functional of the Electron-Density. *Phys. Rev. B* **1988**, *37*, 785−789.
(55) Cances, E.; Mennucci, B.; Tomasi, J. A New Integral Equation Formalism for the Polarizable Continuum Model: Theoretical Background and Applications to Isotropic and Anisotropic Dielectrics. *J. Chem. Phys.* **1997**, *107*, 3032−3041.
(56) Vreven, T.; Byun, K. S.; Komaromi, I.; Dapprich, S.; Montgomery, J. A.; Morokuma, K.; Frisch, M. J. Combining Quantum Mechanics Methods with Molecular Mechanics Methods in ONIOM. *J. Chem. Theory Comput.* **2006**, *2*, 815−826.
(57) Besler, B. H.; Merz, K. M.; Kollman, P. A. Atomic Charges Derived from Semiempirical Methods. *J. Comput. Chem.* **1990**, *11*, 431−439.
(58) Beke, T.; Csizmadia, I. G.; Perczel, A. Theoretical Study on Tertiary Structural Elements of Beta-Peptides: Nanotubes Formed From Parallel-Sheet-Derived Assemblies of Beta-Peptides. *J. Am. Chem. Soc.* **2006**, *128*, 5158−5167.
(59) Jensen, F. An Atomic Counterpoise Method for Estimating Inter- and Intramolecular Basis Set Superposition Errors. *J. Chem. Theory Comput.* **2010**, *6*, 100−106.
(60) Riley, K. E.; Pitonak, M.; Jurecka, P.; Hobza, P. Stabilization and Structure Calculations for Noncovalent Interactions in Extended Molecular Systems Based on Wave Function and Density Functional Theories. *Chem. Rev.* **2010**, *110*, 5023−5063.
(61) Gross, K. C.; Seybold, P. G. Substituent Effects on the Physical Properties and pK_a of Phenol. *Int. J. Quantum Chem.* **2001**, *85*, 569−579.
(62) Destabilization of the negatively charged phenolate ion of MC by the introduction of a less electron withdrawing substituent in *para*-position will increase the corresponding pK_a-value. At the same time, it will increase the rate of the thermal isomerization to the SP isomer. Hence, there is a tradeoff between a high pK_a-value for MCH^+ and good thermal stability of MC.
(63) Shiraishi, Y.; Itoh, M.; Hirai, T. Thermal Isomerization of Spiropyran to Merocyanine in Aqueous Media and its Application to Colorimetric Temperature Indication. *Phys. Chem. Chem. Phys.* **2010**, *12*, 13737−13745.
(64) It has been suggested that SP is converted to *cis*-MCH^+, rather than SPH^+, upon acidification. We believe that this assignment is not valid in our case, as we show that the rate of thermal isomerization to *trans*-MCH^+ is virtually zero for the protonated species. This extreme thermal stability is not consistent with the suggested *cis*-MCH^+ isomer, as it is expected to thermally isomerize to the *trans*-isomer on a much faster time-scale. Note, however, that the kinetic model presented in this study still holds irrespective of the assignment SPH^+ versus *cis*-MCH^+.
(65) Wojtyk, J. T. C.; Wasey, A.; Xiao, N. N.; Kazmaier, P. M.; Hoz, S.; Yu, C.; Lemieux, R. P.; Buncel, E. Elucidating the Mechanisms of Acidochromic Spiropyran-Merocyanine Interconversion. *J. Phys. Chem. A* **2007**, *111*, 2511−2516.
(66) Satoh, T.; Sumaru, K.; Takagi, T.; Takai, K.; Kanamori, T. Isomerization of Spirobenzopyrans Bearing Electron-Donating and Electron-Withdrawing Groups in Acidic Aqueous Solutions. *Phys. Chem. Chem. Phys.* **2011**, *13*, 7322−7329.
(67) Hammarson et al., unpublished results.
(68) Bernasconi, C. F.; Howard, K. A.; Kanavarioti, A. Nucleophilic-Addition to Olefins. 11. Kinetic of the Reversible Hydrolysis of Benzylidenemalonitrile in Water. *J. Am. Chem. Soc.* **1984**, *106*, 6827−6835.
(69) Andraos, J. A Streamlined Approach to Solving Simple and Complex Kinetic Systems Analytically. *J. Chem. Educ.* **1999**, *76*, 1578−1583.
(70) Judging from the excellent fit of the rise and decay curve to a biexponential expression (Figure 3), the condensation reaction is likely to follow first order kinetics. Hence, the rate determining step in this reaction should be of unimolecular nature.
(71) Beke-Somfai, T.; Lincoln, P.; Nordén, B. Mechanical Control of ATP Synthase Function: Activation Energy Difference between Tight and Loose Binding Sites. *Biochemistry* **2010**, *49*, 401−403.
(72) Beke-Somfai, T.; Lincoln, P.; Nordén, B. Double-Lock Ratchet Mechanism Revealing the Role of Alpha SER-344 in FoF1 ATP Synthase. *Proc. Natl. Acad. Sci. U.S.A.* **2011**, *108*, 4828−4833.
(73) Cances, E.; Mennucci, B.; Tomasi, J. A New Integral Equation Formalism for the Polarizable Continuum Model: Theoretical Background and Applications to Isotropic and Anisotropic Dielectrics. *J. Chem. Phys.* **1997**, *107*, 3032−3041.
(74) Warschel, A. In *Computer Modeling of Chemical Reactions in Enzymes and Solutions*; Wiley: New York, 1997.